Unified System- and Circuit-Level Optimization of RES-Based Power-Supply Systems for the Nodes of Wireless Sensor Networks

Ioannis Mandourarakis and Eftichios Koutroulis, *Senior Member, IEEE*

***Abstract*—An extensive utilization of wireless sensor networks has evolved during the last years for monitoring various environmental and artificial processes. When operating in remote locations, the nodes of wireless sensor networks are typically power supplied by an energy production and management system, comprising low-power renewable energy sources, a power electronic converter, and a battery-based energy storage unit. In this paper, a methodology is proposed for optimally designing the energy production and processing system of a wireless sensor network node simultaneously at both the renewable power-supply system level and the power converter circuit level, through a unified design process. The impact of the objective function type on the power-supply design is also investigated in this paper. Design optimization and experimental results are presented, which demonstrate that the optimized power-supply structures derived by applying the proposed optimization technique exhibit lower cost of generated energy compared to partially optimized or totally nonoptimized structures and by that reduce the cost of the overall wireless sensor network node.**

***Index Terms*—DC–DC power conversion, genetic algorithms (GAs), renewable energy sources (RES), sizing optimization, wireless sensor networks (WSNs).**

NOMENCLATURE

DoD	Depth of discharge.
DVS	Dynamic voltage scaling.
GAs	Genetic algorithms.
MAC	Medium access control.
MOSFET	Metal–oxide–semiconductor field-effect transistor.
MPPT	Maximum power point tracking.
MTBF	Mean time between failures.
PSO	Particle swarm optimization.
PV	Photovoltaic.
RES	Renewable energy sources.
SoC	State of charge.
WSN	Wireless sensor network.
W/G	Wind/generator.
C_{Bat}	Total cost of the battery bank.
C_{BATinvst}	Market price of each battery.
$C_{\mathrm{BAT}mntnc}$	Yearly maintenance cost of each battery.
C_{Chr}	Cost of the dc–dc converter.
C_m	Sum of the dc–dc converter components prices.
C_o	Output capacitance of the dc–dc converter.
C_{PS}	Lifetime cost of the power-supply system.
C_{PV}	Total cost of the PV modules.
C_{PVinvst}	Market price of each PV module.
$C_{\mathrm{PV}mntnc}$	Yearly maintenance cost of each PV module.
C_{WT}	Cost of the W/G.
$C_{WT\mathrm{invst}}$	Market price of each W/G.
$C_{WTmntnc}$	Yearly maintenance cost of each W/G.
$C_{WT\mathrm{rod}}$	Cost of the W/G tower per meter of height.
$\mathrm{DoD}_{\max}$	Maximum permissible DoD.
$E_b(t)$	Battery bank energy at hour t of the year.
E_{tot}	Yearly output energy of the dc–dc converter.
H_{inst}	W/G installation height.
$I_{b,c}(t)$	Battery charging current.
$I_{b,d}(t)$	Battery discharging current.
$I_{\max,c}$	Maximum permissible charging current.
$I_{\max,d}$	Maximum permissible discharging current.
$I_o(t)$	Output current of the dc–dc converter at hour t.
I_p	Peak current of the power MOSFETs.
$I_{p,\max}$	Maximum limit of the MOSFETs peak current.
L	Inductance of the dc–dc converter.
LCOE	Levelized cost of the electricity generated.
N_{BAT}	Total number of batteries.
N_{bp}	Number of battery strings connected in parallel.
N_{bs}	Number of batteries connected in series.
N_p	Number of power MOSFETs connected in parallel.
N_{pv}	Total number of PV modules.
$P_b(t)$	Total power flowing to the battery bank.
P_C	Total power loss of the remaining components.
$P_{C\mathrm{out}}$	Power loss of the output capacitor.
P_{Diode}	Power loss of the diode.
P_{Inductor}	Power loss of the inductor.
P_L	Total power loss of the dc–dc power converter.

Manuscript received May 16, 2017; revised July 12, 2017 and August 24, 2017; accepted August 30, 2017. Date of publication September 13, 2017; date of current version February 1, 2018. This work was supported by the SYN11-6-925 AquaNet project, which was executed within the framework of the "Cooperation 2011" program of the Greek General Secretariat for Research & Technology, funded through European Union and national funds. Paper no. TII-17-1047. *(Corresponding author: Eftichios Koutroulis.)*

The authors are with the School of Electrical and Computer Engineering, Technical University of Crete, Chania 73 100, Greece (e-mail: i.mandourarakis@gmail.com; efkout@electronics.tuc.gr).

Color versions of one or more of the figures in this paper are available online at http://ieeexplore.ieee.org.

Digital Object Identifier 10.1109/TII.2017.2751749

P_{MOSFET}	Power loss of the MOSFETs.
P_o	DC–DC converter output power.
$P_{\mathrm{pv}}(t)$	MPPT power of the PV modules at hour t.
$RF_{o,c}$	Output current ripple.
$RF_{\max}$	Maximum limit of the output current ripple.
$\mathrm{SoC}(t)$	Battery bank SoC at hour t of the year.
$\overline{T_A}$	Weighted-average value of ambient temperature.
V_b	Nominal voltage of each battery.
$\overline{V_{\mathrm{out}}}$	Weighted-average value of the output voltage.
$\boldsymbol{X_s}$	Vector of design variables.
Y	Planned lifespan of the RES system under design.
f_s	Switching frequency of the dc–dc converter.
$f_{s,\max}$	Maximum limit of the switching frequency.
n	Efficiency of the dc–dc converter.
n_b	Battery round-trip efficiency.
β	PV modules tilt angle.
Δt	Simulation time step.
$\lambda_{C\mathrm{out}}$	Output capacitor failure rate.
λ_{diode}	Diode failure rate.
$\lambda_{\mathrm{inductor}}$	Inductor failure rate.
$\lambda_{\mathrm{MOSFET}}$	Failure rate of each power MOSFET.
λ_{rest}	Failure rate of the remaining components.
λ_{SUM}	Total failure rate of the dc–dc converter.

I. Introduction

NOWADAYS, WSNs are widely installed for monitoring the environment, as well as residential and industrial processes. Simultaneously, modern applications of WSNs, such as the Internet of Things, Smart Grids, etc., are also evolving [1]. A block diagram of a WSN node power production and management system is depicted in Fig. 1. Usually, the electronic circuits (i.e., sensors, wireless transceivers, etc.) comprising the WSN nodes are required to operate in remote areas, where, due to the lack of conventional electric power, they are power supplied by low-power RES, such as PVs and W/Gs. Also, energy storage devices, typically in the form of batteries, are used to store any RES-generated energy surplus in order to be used during time periods with low RES energy production. The power-supply systems of WSN nodes are required to exhibit low manufacturing and lifetime maintenance costs, in order to reduce the cost of the overall WSN which contains a large number of sensing nodes installed at different locations. Therefore, the RES-based power-supply systems for WSN nodes typically comprise a unique power-source type (i.e., either PV modules or a W/G) with a low-power rating. Thus, it is essential to optimally exploit the available RES energy. The RES-generated energy is interfaced to the battery bank through a dc–dc converter, which is controlled by a microcontroller- or DSP-based control unit, in order to: 1) execute a MPPT process for extracting the maximum possible power under the continuously varying meteorological conditions (i.e., solar irradiation, ambient temperature, and wind speed) [2]; and 2) regulate the battery charging process such that battery overcharging is avoided [3]. As illustrated in Fig. 1, two different levels of design, each with particular objectives, must be accomplished in order to synthesize the power-supply system of the WSN node: 1) the system-level design, where the types,

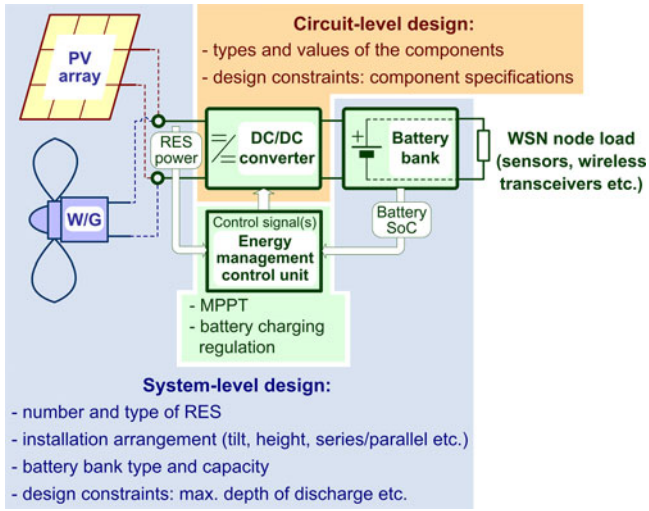

Fig. 1. Block diagram of a RES-based power-supply system for WSN nodes.

power capacities, and installation arrangement (e.g., tilt angle of PV modules, height of the W/G, number of batteries connected in series/parallel, etc.) of the energy production and storage units must be decided, a such that the energy requirements of the electric load of the WSN node are completely covered during the entire year; and 2) the circuit-level design of the dc–dc converter, where the values and types of the components used to build the power converter circuit are calculated. The design process in each of these levels is performed subject to the corresponding constraints (e.g., maximum permissible values of the battery bank DoD and of the switching frequency of the dc–dc converter power semiconductors, etc.). Also, the overall design process should ensure that the resulting power-supply system exhibits the minimum possible cost.

Prior research on energy management of WSNs that are power supplied by harvesting ambient energy has been focused on the development of energy-aware routing protocols, MAC protocols, duty-cycling strategies for activating and deactivating the WSN nodes, as well as the optimization of the data transmission rate and the transmission power level [4]–[7]. In [8], an algorithm is presented for dynamically reconfiguring the hardware of the data-processing unit (e.g., for video processing, execution of encryption algorithms, etc.) that is embedded in a WSN node equipped with energy-harvesting sources, such that its energy consumption is minimized. Alternatively, a DVS scheme may also be used for reducing the WSN node power consumption, by adjusting (in real-time) the power-supply voltage and clock frequency of the data-processing unit [9]. The target of the aforementioned techniques is to minimize the energy-exhaustion events of the WSN nodes and, simultaneously, ensure that the necessary information is always transferred on-time to the end-user application, thus enhancing the reliability of the overall WSN. Therefore, the application of these techniques only affects the energy consumption of the electric load of the WSN node that is depicted in Fig. 1. The design of the WSN node power-supply system (also shown in Fig. 1), where the work proposed in this paper is focused on, is typically

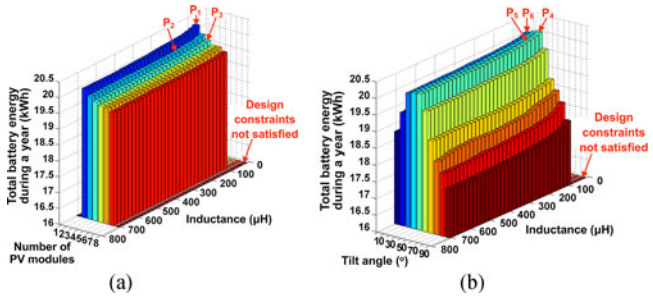

Fig. 2. Variation of the total annual energy transferred to a 12 V battery bank through a step-up dc/dc converter: (a) versus the total number of PV modules and the dc/dc converter inductance and (b) versus the tilt angle of the PV modules and the dc/dc converter inductance.

considered as a design task of a conventional RES-based energy production system. Such a RES-based power-supply system is designed to satisfy the (*a priori* known) energy consumption of the WSN node electric load and, till present, the methods described in the following paragraph have been developed for its design.

Plenty of system-level design optimization techniques for RES-based power supplies are available in the existing research literature [10]–[14]. These techniques have been applied for calculating the optimal numbers of PVs, W/Gs and energy storage units that compose, either stand-alone or grid-connected, PV or hybrid PV/wind systems. They have been implemented by applying optimization techniques such as the PSO or the fuzzy-adaptive GAs, in order to minimize the total cost of the energy production system and maximize its reliability. These design methods do not take into account the impact of the circuit-level design of the power converter(s) that they comprise (see Fig. 1), on the efficiency and cost of the overall RES-based power-supply system. Furthermore, optimization techniques have been developed for the circuit-level design of PV power converters [15]–[20], which, due to the variability of meteorological conditions, are required to operate under continuously changing dc-input power and voltage levels. These design methods have been used to calculate the optimal values of design parameters such as the switching frequency, inductance value, etc., by employing performance metrics such as the efficiency, power density, and reliability as objective functions of the optimization process. However, all of the aforementioned design techniques of RES-based power-supply systems have been focused exclusively on either the system-, or the circuit-level design (see Fig. 1), without considering the interdependence of these two design stages and the impact of that interdependence on the energy production performance and cost of the overall power-supply system. In order to demonstrate the importance of that drawback, an example of the variation of the total annual energy transferred to a 12 V battery bank through a step-up dc/dc converter (see Fig. 1), versus the total number of PV modules and the dc/dc converter inductance, which constitute major system- and circuit-level design parameters, is presented in Fig. 2(a). The overall annual energy is maximized at point P_1. At points P_2 and P_3, approximately equal amounts of annual energy are transferred to the battery bank, although different numbers of PV modules and dc/dc converter inductance values are combined at each point. However, the total cost of the PV system is higher for point P_3 due to the higher cost of PV modules. A similar effect is observed in the characteristic of the battery bank annual energy versus the PV modules tilt angle and the dc/dc converter inductance. As shown in Fig. 2(b), in that case, approximately equal amounts of energy are transferred to the battery bank at points P_5 and P_6, despite that a different mixture of values of the system- and circuit-level design parameters is applied for each of these points. The total energy is maximized for the tilt angle and inductance values that correspond to point P_4. The results presented in Fig. 2 demonstrate that in order to maximize the energy production of the RES-based power-supply system, both the system- and the circuit-level design parameters must simultaneously be considered during the execution of the design process. However, this aspect is not taken into account by the existing design methods of RES-based power supplies that have been described above, since they focus exclusively on either the system- or the circuit-level design.

Hence, targeting to fill this gap, design techniques which initially had been developed for designing RES-based power supplies for WSN nodes only at the system-level [21] and only at the circuit-level [22], respectively, are further evolved in this paper in order to comprise an integrated design methodology for optimally codesigning the power-supply system of a WSN node (see Fig. 1) simultaneously at both the RES-system and the dc–dc converter circuit levels, through a unified design process. The mission profile of the RES system, in terms of the yearly meteorological conditions at the installation site and the load demand of the WSN node, are also considered in the proposed optimization process. The scientific contributions of the proposed research work are the following.

1) To the authors' knowledge, this is the first time in the existing literature that a technique is presented for the optimal codesign of a RES-based power-supply structure, simultaneously at the RES system-level and the dc–dc converter circuit level.
2) The impact of the objective function type on the design optimization results of the RES-based power-supply system is also investigated for the first time in this paper.
3) In contrast to the past-proposed design approaches, which are focused exclusively on either the RES system design, or the power-converter circuit design, the proposed methodology enables to optimally explore the trade-off between the operational characteristics of the power production/processing structures designed at each of these two distinct design levels.
4) As will be demonstrated through the design optimization and experimental results presented in this paper, the proposed method enables the reduction of the cost of the energy produced by the power-supply system of the WSN node, compared to that of partially optimized (i.e., subject only to system-level optimization), or totally nonoptimized RES-based power-supply structures and, therefore, the cost of the entire WSN can be reduced accordingly.

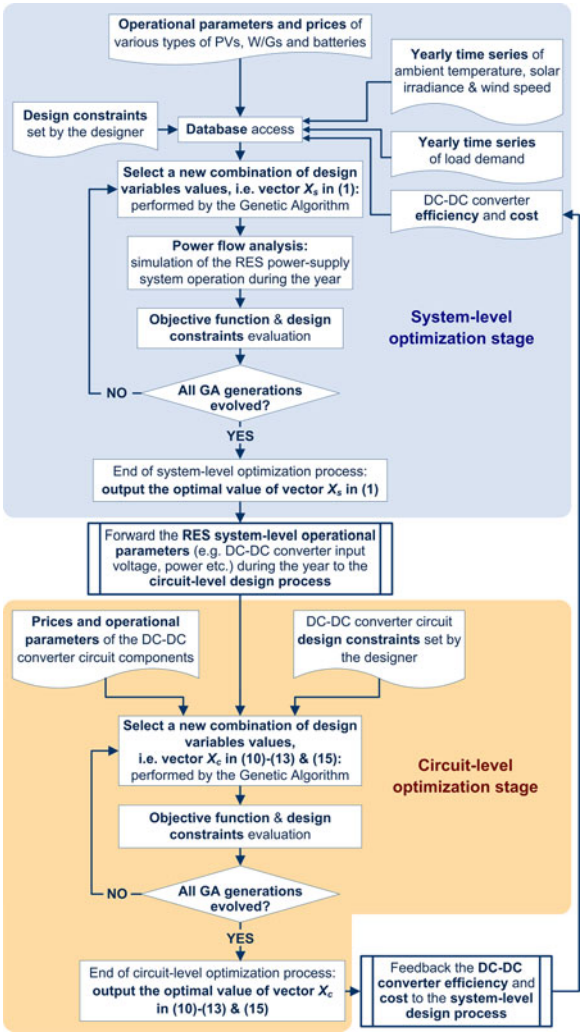

Fig. 3. Flowchart of the proposed optimization method for RES-based power-supply systems of WSN nodes.

This paper is organized as follows: the proposed design optimization methodology is described in Section II; the design optimization results are analyzed in Section III, and the experimental results are presented in Section IV; finally, the conclusions are discussed in Section V.

II. Proposed Design Optimization Methodology

A flowchart of the proposed optimization method is depicted in Fig. 3. In order to incorporate into the proposed optimization method the interdependence between the system- and circuit-level design processes, the proposed technique comprises two stages executed iteratively: initially, a system-level optimal design of the RES-based power supply of the WSN node (see Fig. 1) is performed for calculating the optimal value of the vector of the system-level design variables, $\boldsymbol{X_s}$, which also determines the operating conditions of the dc–dc converter (e.g., input and output voltage and current, etc.) and then the configuration of the dc–dc converter circuit that this system comprises is optimized by deriving the optimal value of the circuit-level design variables vector, $\boldsymbol{X_c}$. The circuit-level design results are then fed-back to the system-level stage and the previous process is iteratively repeated until a dc–dc converter efficiency value is produced by the circuit-level design optimization stage, which does not differ by more than 1% from its previous value. The resulting values of $\boldsymbol{X_s}$ and $\boldsymbol{X_c}$ comprise the set of optimal values of the design parameters of the entire power-supply system. The vectors $\boldsymbol{X_s}$ and $\boldsymbol{X_c}$ are defined in the following paragraphs, together with an analytical description of the two aforementioned stages of the proposed optimization process.

A. System-Level Optimization Stage

In contrast to the grid-connected PV systems, where it is important to maximize the total energy production during the year and, for that purpose, the PV modules tilt angle is conventionally set close to the latitude angle of the installation site, the nodes of WSNs comprise stand-alone RES systems (i.e., not connected to the electric grid), which is desirable to exhibit the minimum possible cost and ensure that the load is power supplied continuously. Thus, the target of the proposed system-level design stage is to compute the optimal type and number of the RES energy production devices (i.e., an array of PV modules or a single W/G) and battery energy-storage units comprising the RES-based power-supply system of the WSN node, as well as their optimal installation arrangement. The latter includes the number of batteries to be connected in series and/or in parallel, the PV modules tilt angle and the height of the W/G.

The configuration of the RES system determines the input and output voltage ranges of the dc–dc converter circuit, which, in turn, affect the dc–dc converter efficiency. This characteristic is also considered in the proposed optimization methodology during the circuit-level design stage, as described next. The inputs of the system-level optimization stage are the following (see Fig. 3).

1) The prices and operational parameters of commercially available RES system devices (e.g., open-circuit voltage and short-circuit current of PV modules, nominal voltage of batteries, etc.), provided in the respective manufacturer datasheets.
2) The time-series of hourly average values of solar irradiation, ambient temperature, and wind speed that prevail at the installation site of the WSN node during the year.
3) The time-series of the power consumption of the WSN node electric load during the year.
4) The design constraints, such as the maximum permissible DoD and maximum permissible charging/discharging currents of the batteries.

The dc–dc converter efficiency and cost are fed-back from the circuit-level optimization stage, as described next.

The system-level optimization process calculates the optimal values of the design variables which: 1) minimize the lifetime cost of the RES-based power-supply system; 2) ensure that the electric energy requirements of the WSN node electric load (i.e., sensors, wireless transceivers, etc.) are uninterruptedly satisfied during the entire year; and 3) satisfy the design constraints imposed by the system designer. The lifetime cost of the power-supply system, C_{PS} (€), is calculated as analyzed

in [21], considering both the capital and maintenance costs of the devices comprising the power-supply system:

$$C_{\mathrm{PS}}\left(\boldsymbol{X_s}\right) = C_{\mathrm{PV}} + C_{Chr} + C_{\mathrm{Bat}} \text{ or}$$
$$C_{\mathrm{PS}}(\boldsymbol{X_s}) = C_{WT} + C_{Chr} + C_{\mathrm{Bat}} \quad (1)$$

where

$$C_{\mathrm{PV}} = (C_{\mathrm{PVinvst}} + Y \cdot C_{\mathrm{PV}mntnc}) \cdot N_{\mathrm{pv}} \quad (2)$$
$$C_{WT} = C_{WT\mathrm{invst}} + C_{WT\mathrm{rod}} \cdot H_{\mathrm{inst}} + Y \cdot C_{WTmntnc} \quad (3)$$
$$C_{\mathrm{Bat}} = (C_{\mathrm{BATinvst}} + Y \cdot C_{\mathrm{BAT}mntnc}) \cdot N_{\mathrm{BAT}} \quad (4)$$

and $\boldsymbol{X_s}$ is the vector of design variables whose optimal values are calculated by the system-level optimization process, where $\boldsymbol{X_s} = [N_{\mathrm{pv}}, N_{\mathrm{BAT}}, \beta, N_{bs}, N_{bp}]$ in case that the power-supply system is based on PV modules, else $\boldsymbol{X_s} = [N_{\mathrm{BAT}}, H_{\mathrm{inst}}, N_{bs}, N_{bp}]$, C_{PV} (€) is the total cost of the PV modules, C_{WT} (€) is the cost of the W/G, C_{Chr} (€) is the cost of the dc–dc converter, C_{Bat} (€) is the total cost of the battery bank, C_{PVinvst}, $C_{WT\mathrm{invst}}$, and C_{BATinvst} (€) are the market prices of each PV module, W/G and battery, respectively, $C_{\mathrm{PV}mntnc}$, $C_{WTmntnc}$, and $C_{\mathrm{BAT}mntnc}$ (€/year) are the yearly maintenance costs of each PV module, W/G and battery, respectively, Y (years) is the planned lifespan of the RES system under design, $C_{WT\mathrm{rod}}$ (€/m) is the cost of the W/G tower per meter of height, H_{inst} (m) is the W/G installation height, N_{pv}, N_{BAT} are the total number of PV modules and batteries, respectively, β (°) is the PV modules tilt angle, N_{bs} is the number of batteries connected in series, and N_{bp} is the number of battery strings connected in parallel for forming the battery bank of the WSN node. The yearly maintenance cost of each battery [i.e., parameter $C_{\mathrm{BAT}mntnc}$ in (4)] is equal to the sum of the annual inspection/repair cost (e.g., for cabling, connectors, etc.) and the cost of replacing the battery if the end of its service lifetime period due to aging has been reached. The batteries replacement cost is calculated as analyzed in [13].

In order to achieve the design targets 1–3 described above, the selection of the PV modules tilt angle must be based on an analysis of the time-series of solar irradiation at the target installation site during the entire year, since, e.g., by reducing the value of the PV modules tilt angle increases the diffuse irradiation received by the PV generator surface, which is the main component of the incident solar irradiation under cloudy conditions. Simultaneously, increasing the size of the energy storage unit enables to store higher amounts of PV-generated surplus energy that is available during time periods with high solar irradiance availability, but this also increases the cost of the PV system. Thus, in the proposed optimization technique, the tilt angle has been set to be a decision variable of the system-level optimization process, together with the sizes of the energy production and storage units of the PV system. Also, in order to investigate whether the electric load energy requirements are satisfied for any given set of design variables values (i.e., vector $\boldsymbol{X_s}$), the operation of the WSN node energy production system is simulated for a time period of one year with a time step of 1 h. During that simulation process, the output power of the RES source is calculated for a time period of one year. In case that a PV array is used, its power production is calculated by using an appropriate solar irradiance model [23] and processing the solar irradiation and ambient temperature time-series that are provided by the designer. The resulting time-series of RES power generation is provided to a power-flow algorithm which, given a particular energy storage configuration, estimates for every time-step during the year (i.e., 1 h) the corresponding SoC of the battery bank. During the simulation process, the usable energy, $E_b(t)$, that is stored in the battery bank at hour t of the year (i.e., $1 \leq t \leq 8760$), is calculated as follows [21]:

$$E_b(t) = E_b(t-1) + n_b \cdot P_b(t) \cdot \Delta t \quad (5)$$

where n_b (%) is the battery round-trip efficiency (it has been considered that $n_b = 81\%$ during charging and $n_b = 100\%$ during discharging), $P_b(t)$ is the total power flowing to the battery bank [i.e., $P_b(t) < 0$ during discharging and $P_b(t) > 0$ during charging], and $\Delta t = 1$ h is the simulation time-step.

The proposed optimization process is executed subject to the following constraints, which must be fulfilled at each hour t of the year ($1 \leq t \leq 8760$):

$$\mathrm{SoC}(t) \geq 1 - \mathrm{DoD}_{\max} \quad (6)$$
$$I_{b,c}(t) \leq I_{\max,c} \quad (7)$$
$$I_{b,d}(t) \leq I_{\max,d} \quad (8)$$

where $\mathrm{SoC}(t)$ is the battery bank SoC at hour t of the year (i.e., $1 \leq t \leq 8760$), $\mathrm{DoD}_{\max}$ is the maximum permissible DoD, $I_{b,c}(t)$ and $I_{b,d}(t)$ are the charging and discharging currents of the batteries and $I_{\max,c}$ (A), $I_{\max,d}$ (A) are the maximum permissible charging and discharging currents, respectively, specified by the battery manufacturer. The charging/discharging current of the batteries [i.e., $I_{b,c}(t)$ and $I_{b,d}(t)$ in (7) and (8)] is calculated by

$$I_{b,c/d}(t) = \frac{P_b(t)}{N_{bp} \cdot N_{bs} \cdot V_b} \quad (9)$$

where V_b is the nominal voltage of the individual batteries comprising the battery bank.

In order to calculate the optimal value of the objective function of the system-level design stage [given by (1)] and the corresponding vector of optimal values of the design variables [i.e., $\boldsymbol{X_s}$ in (1)], GAs have been employed due to their computational efficiency in complex optimization problems [24]. The GA execution is repeated until a predefined number of generations have evolved. By using GAs, the calculations in (1)–(9) are repeated for multiple alternative values of the decision variables [i.e., $\boldsymbol{X_s}$ in (1)]. Through this process, the optimal values of tilt angle and energy production/storage capacities can be derived, such that the total cost of the RES system is minimized and the uninterruptible power supply to the load of the WSN node during the entire year is ensured. Given the optimal configuration of the RES-based power-supply system derived by the system-level design phase, as analyzed above, the input/output voltage and current levels of the dc–dc converter during the entire year are calculated next and the corresponding results are forwarded to the circuit-level design stage, which is described in the following paragraph.

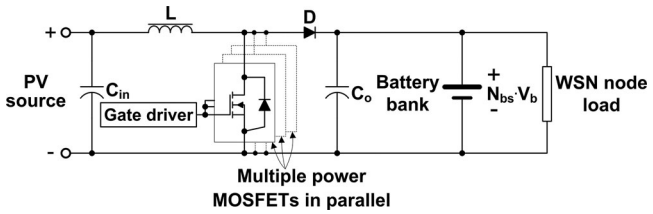

Fig. 4. Circuit diagram of a boost-type dc–dc converter.

B. Circuit-Level Optimization Stage

In this work, it has been assumed that a boost-type dc–dc converter (see Fig. 4) is employed to interface the RES-generated energy to the battery bank and the electric load of the WSN node. However, the proposed technique is also applicable to any dc–dc converter topology. The inputs initially provided by the designer to the circuit-level optimization stage are the following (see Fig. 3).

1) The prices and operational parameters of commercially available electronic components (e.g., on-state voltage of diodes, resistance of power MOSFETs, etc.), which are provided in the respective manufacturer datasheets.
2) The constraints that should be considered during the dc–dc converter design, which are expressed by (16)–(18) as discussed in the following.

With reference to the circuit diagram depicted in Fig. 4, the following parameters, mainly contributing to the total power loss and cost of the dc–dc converter circuit, have been selected to comprise the set of design variables of the circuit-level optimization process: the number of power MOSFETs connected in parallel N_p, as well as their switching frequency f_s, the inductance L, and the output capacitance C_o. These parameters form the vector of design variables of the circuit-level optimization stage, i.e., $\boldsymbol{X_c} = [f_s, N_p, L, C_o]$. The target of that stage is to compute the optimal value of $\boldsymbol{X_c}$, which results in the minimization or maximization, respectively, of the preselected performance metric of the dc–dc power converter, while, simultaneously, guaranteeing that the desired design constraints are satisfied, as described next.

Four performance metrics have been considered as alternative objective functions of the proposed optimization process. The first type of objective function is the efficiency of the dc–dc converter, n, under nominal output power conditions:

$$n(\boldsymbol{X_c}) = \frac{P_o}{P_{\rm pv}} = \frac{P_o}{P_o + P_L} \tag{10}$$

where $P_{\rm pv}$ is the total power produced by the PV modules under MPPT conditions, P_o is the dc–dc converter nominal output power flowing to the battery bank and the electric load of the WSN node, and P_L is the total power loss of the boost-type dc–dc power converter.

The value of P_L in (10) is calculated as follows [22]:

$$P_L(\boldsymbol{X_c}) = P_{\rm MOSFET} + P_{\rm Diode} + P_{\rm Inductor} + P_{C\rm out} + P_C \tag{11}$$

where $P_{\rm MOSFET}$ and $P_{\rm Diode}$ are the total conduction and switching losses of the power MOSFETs and diode, respectively, $P_{\rm Inductor}$ and $P_{C\rm out}$ (W) are the power losses of the inductor and output capacitor, respectively, and P_C is the total power loss of the input capacitor, printed circuit board (PCB) conductors and MOSFET gate-drive circuits of the dc–dc converter.

In order to maximize n, the minimum value of P_L is calculated with (11). The value of P_L is calculated as analyzed in [22], by using the information provided in the manufacturer datasheets of the components used to construct the dc–dc converter circuit.

The second alternative performance metric is the yearly energy loss of the dc–dc converter, which is calculated as follows [22]:

$$E_{L,\rm tot}(\boldsymbol{X_c}) = \sum_{t=1}^{8760} P_L(t) \cdot \Delta t \tag{12}$$

where $P_L(t)$ is the total power loss of the dc–dc converter at hour t ($1 \le t \le 8760$) and $\Delta t = 1$ h is the time-step.

The third type of objective function is the LCOE, which is given by

$$\text{LCOE}(\boldsymbol{X_c}) = \frac{C_m}{E_{\rm tot}} = \frac{C_m}{\sum_{t=1}^{8760} [P_{\rm pv}(t) - P_L(t)] \cdot \Delta t} \tag{13}$$

where C_m (€) is the sum of the prices of the individual components comprising the dc–dc converter circuit, $E_{\rm tot}$ is the yearly output energy of the dc–dc converter, and $P_{\rm pv}(t)$ is the total output power of the PV modules at hour t ($1 \le t \le 8760$). The total power loss P_L in (10)–(13) is calculated as described in [22], by also considering that the following power-balance equation must be satisfied for each value of PV-generated power, $P_{\rm pv}$, during each hour t ($1 \le t \le 8760$) of the year:

$$P_{\rm pv}(t) = P_L(t) + N_{bs} \cdot V_b \cdot I_o(t) \tag{14}$$

where $I_o(t)$ is the output current of the dc–dc converter at hour t, which is provided to the battery bank and the WSN node load.

Finally, the use of the total failure rate of the dc–dc converter has also been considered as an objective function of the circuit-level optimization process. The dc–dc converter total failure rate, $\lambda_{\rm SUM}(\boldsymbol{X_c})$ (number of failures/10^6 h), is calculated for each set of the design variables values (i.e., $\boldsymbol{X_c} = [f_s, N_p, L, C_o]$) examined during the execution of the proposed optimization process, by using the following equation:

$$\lambda_{\rm SUM}(\boldsymbol{X_c}) = \lambda_{C\rm out}\left(\overline{V_{\rm out}},\ \overline{T_A}\right) + \lambda_{\rm inductor}\left(\overline{T_A}\right) + N_p \cdot \lambda_{\rm MOSFET}\left(\overline{T_A}\right) + \lambda_{\rm diode}\left(\overline{T_A}\right) + \lambda_{\rm rest} \tag{15}$$

where $\lambda_{C\rm out}$ is the output capacitor failure rate, $\lambda_{\rm inductor}$ is the inductor failure rate, $\lambda_{\rm MOSFET}$ is the failure rate of each power MOSFET, $\lambda_{\rm diode}$ is the diode failure rate, $\lambda_{\rm rest}$ is the total failure rate of the remaining components (e.g., microcontroller, control circuit, PCB, etc.), $\overline{T_A}$ is the weighted-average value of the dc–dc converter ambient temperature, and $\overline{V_{\rm out}}$ is the weighted-average value of the dc–dc converter output voltage. The values of $\lambda_{C\rm out}$, $\lambda_{\rm inductor}$, $\lambda_{\rm MOSFET}$, and $\lambda_{\rm diode}$ are calculated according to [25] and the value of $\lambda_{\rm rest}$ is considered to be constant.

The MTBF of the dc–dc converter is equal to the inverse of $\lambda_{\mathrm{SUM}}(\boldsymbol{X_c})$ [26].

In the circuit-level optimization stage, the optimal values of the design variables (i.e., vector $\boldsymbol{X_c} = [f_s, N_p, L, C_o]$) are derived using GAs such that the desired objective function [i.e., (10), (12), (13), or (15), respectively] is optimized [i.e., $n(\boldsymbol{X_c})$ is maximized and $E_{L,\mathrm{tot}}(\boldsymbol{X_c})$, $\mathrm{LCOE}(\boldsymbol{X_c})$, $\lambda_{\mathrm{SUM}}(\boldsymbol{X_c})$ are minimized]. The optimization process is performed subject to the following design constraints.

1) The output current ripple, $RF_{o,c}$, is less than the maximum permitted limit, $RF_{\max}$:

$$RF_{o,c} \leq RF_{\max}. \tag{16}$$

2) The peak current that flows through the power MOSFETs, I_p, is less than the maximum permitted limit, $I_{p,\max}$:

$$I_p \leq I_{p,\max}. \tag{17}$$

3) The switching frequency is less than the maximum permitted limit, $f_{s,\max}$:

$$f_s \leq f_{s,\max}. \tag{18}$$

The values of $RF_{\max}$, $I_{p,\max}$, and $f_{s,\max}$ are specified by the designer at the beginning of the circuit-level optimization stage according to the components specifications provided in the manufacturer datasheets.

III. Design Results

The optimal design of the RES-based power-supply system of a WSN node, which belongs to a city-wide wireless network located in the area of Chania (Greece) [27], was performed as a case study. The WSN node under consideration contains an electric load drawing continuously (i.e., for 24 h per day/365 days per year) approximately 3 W at 12 V, corresponding to the total power consumption of the WSN node sensor, signal-conditioning circuits, data-processing computer board, and wireless transceiver. This power consumption value was provided as input to the system-level design stage of the proposed optimization process as discussed in Section II-A, since it affects the structure and lifetime cost of the RES system that is required to ensure an uninterruptible power supply to the electric load during the entire year. The proposed design process described in Section II has been implemented in the form of a MATLAB-based software program in order to calculate the optimal values of vector $\boldsymbol{X_s}$ in (1) and $\boldsymbol{X_c}$ in (10), (12), (13), or (15), respectively. The GA ability to derive the global optimum solution in the optimization problem under study, instead of converging to local optima, was verified through an exhaustive-search process, which, however, requires a significantly longer time period in order to be accomplished. The operational characteristics and prices of commercially available circuit components and RES system devices have been considered during the execution of the proposed optimization process, as described in Section II: the system-level design phase has been implemented considering commercially available 20 W/6 V monocrystalline PV modules, a W/G with a 30 W nominal power rating, as well as 7 A·h lead-acid batteries with $V_b = 12\,\mathrm{V}$, $\mathrm{DoD}_{\max} = 80\%$, $I_{\max,c} = 2.1\,\mathrm{A}$, and $I_{\max,d} = 12\,\mathrm{A}$ in (6)–(8); the dc–dc converter has been designed through the circuit-level design phase, considering the PSMN2R2-40PS power MOSFETs and STTH61W04S diode, with $RF_{\max} = 1\%$, $I_{p,\max} = 90\,\mathrm{A}$, and $f_{s,\max} = 400\,\mathrm{kHz}$ in (16)–(18).

TABLE I
Design Optimization Results for Alternative Objective Functions of the Circuit-Level Optimization Process

Design parameter	Objective function	
	Efficiency maximization	Reliability maximization
Inductance (L)	0.095 mH	2.164 mH
Output capacitance (C_o)	3.077 mF	0.015 mF
Switching frequency (f_s)	128.4 kHz	53.6 kHz
Number of MOSFETs (N_p)	1	1
MTBF (only for the components with an optimization-dependent failure rate)	5.76 years	5.78 years
Total energy loss during the year	4.63 kW·h	13.76 kW·h
Cost of corresponding components	17.68 €	58.84 €

The optimization results that are produced in case that the objective function of the circuit-level optimization process is alternatively either the efficiency at maximum output power, or the total failure rate of the dc–dc converter, are presented in Table I. It is observed that, depending on the type of objective function employed in the optimization process, the GA process favored a different combination of optimal values of the design variables. Also, the design results presented in Table I indicate that by employing the total failure rate as an objective function then the optimization-dependent part of the MTBF is improved by only 0.35%, but the dc–dc converter annual energy loss and total cost of the corresponding components are significantly increased by 297.2% and 332.8%, respectively. These percentages resulted because a higher optimal value of inductance and a lower optimal value of output capacitance were derived (see Table I) when the dc–dc converter reliability was applied as an objective function of the circuit-level optimization phase, compared to the corresponding values produced by the efficiency maximization process, since: 1) the power loss of the inductor does not significantly affect the value of the reliability-based objective function, which is calculated according to [25] as analyzed in Section II-B; and 2) by reducing the size of the output capacitor, which is a less reliable component, contributes to the reduction of the dc–dc converter total failure rate. In contrast, the optimal switching frequency is higher in the case of optimization for achieving maximum efficiency, because this enabled to reduce the size of the dc–dc converter inductance, which, in turn, resulted in a reduction of the inductor power loss. Therefore, this approach enabled to reduce the total power loss of the dc–dc converter and increase its efficiency, since, for the operational characteristics of the specific circuit components considered in this design example (provided in the manufacturer datasheets), the power loss of the inductor dominates over the power losses of the MOSFET and diode (despite the fact that their losses increase with switching frequency). Thus, according to the results presented in Table I, by employing reliability as a performance metric of the circuit-level optimization process, does not significantly

TABLE II
CIRCUIT- AND SYSTEM-LEVEL CONFIGURATIONS OF THE POWER-SUPPLY SYSTEMS UNDER EVALUATION

	Optimized at both the system and circuit design levels		Partially optimized	Nonoptimized
Design variables	#1: optimized for efficiency and total lifetime cost	#2: optimized for LCOE and total lifetime cost	#3:	#4:
CL: number of MOSFETs (N_p)	1	1	1	1
CL: L (μH)	100 μH	75 μH	300 μH	300 μH
CL: C_o (mF)	3.0 mF	3.0 mF	3.0 mF	3.0 mF
CL: f_s (kHz)	129 kHz	242 kHz	63 kHz	63 kHz
SL: optimal type of energy source	PVs	PVs	PVs	PVs
SL: number of PV modules (N_{pv})	2	2	2	3
SL: PV modules tilt angle (β)	28°	28°	28°	60°
SL: number of batteries (N_{BAT})	4	4	4	4

"CL" stands for circuit-level and "SL" for system-level design.

improve the dc–dc converter MTBF, while simultaneously, the energy production performance and cost of the dc–dc converter are negatively affected. These results also demonstrate the ability of the proposed automated design methodology to produce design results that, although seem counterintuitive if the conventional design approaches are followed, enable the actual optimization of the RES-based power system design.

The proposed optimization method was also applied for deriving the optimal values of the design variables, when employing the total lifetime cost [given by (1)] as objective function of the system-level design stage and the efficiency at maximum power [given by (10)] and LCOE [given by (13)], respectively, as objective functions of the circuit-level design stage of the proposed optimization process. The corresponding optimization results, in terms of the optimal values of the design variables at both the system and circuit levels, are presented in Table II. It is observed that PV modules instead of a W/G have been derived by the proposed design process as the optimal energy source type for the WSN node. This result arises since the use of a W/G (even of low nominal power rating) significantly increased the lifetime cost of the power-supply system due to the low wind speed potential of the target installation site under consideration.

IV. EXPERIMENTAL RESULTS

Fully functional experimental prototype systems were designed and constructed according to the design optimization results presented in Table II (using commercially available components with the closest values possible) for power supplying the WSN node under consideration. In order to evaluate the benefits offered by the proposed optimization technique, nonoptimized structures of the dc–dc converter circuit and RES-based power-supply system were also designed and constructed. The resulting parameters are also presented in Table II, where configuration #3 has been partially optimized by including a nonoptimized dc–dc converter circuit in an optimized system-level design, while configuration #4 has not been optimized at either the system or the circuit level (i.e., totally nonoptimized). The values of the design variables employed in the system- and circuit-level nonoptimized structures of configurations #3 and #4 have been calculated by using conventional design techniques [23], [28], so that the same design constraints of the proposed optimization process are also satisfied, but without optimizing the corresponding performance metrics [i.e., objective functions (1), (10), (12), (13), or (15), respectively]. In the totally nonoptimized configuration #4, the tilt angle has been set such that the total solar irradiation incident on the PV modules during December and January is maximized [23]. These months correspond to the time period of the year with the lowest solar irradiation potential at the target installation site under consideration. In contrast to the proposed methodology, when applying this (conventional) design approach [23], simulations of the PV system operation during each hour of the year for various alternative values of the design parameters (e.g., number of PV modules, battery bank capacity, etc.), are not performed. Therefore, the resulting RES-based power supplies exhibit a higher lifetime cost. Photographs of one of the PV-based power-supply system comparison setups and one of the dc–dc converter circuits that were employed are illustrated in Fig. 5.

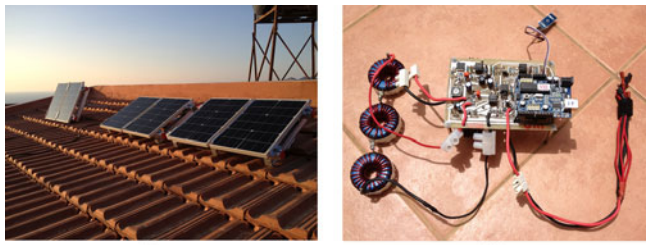

Fig. 5. Examples of prototype systems employed in the experimental performance evaluation process: (a) RES-based power-supply system comparison setups and (b) dc–dc converter with 300 μH inductance and 63 kHz switching frequency.

Experiments were conducted with a total duration of 382.5 h of operation, such that the energy production performance of the optimized, partially optimized and nonoptimized configurations presented in Table II is investigated under various solar irradiation and ambient temperature conditions. Example plots of the power provided by the dc–dc converter to the battery bank and load for the power-supply configurations subject to the experimental evaluation process (i.e., Table II) during the aforementioned experimental tests, are shown in Fig. 6. In all experimental configurations, a 3 W/12 V resistor array has been connected as a load at the battery bank terminals. During the

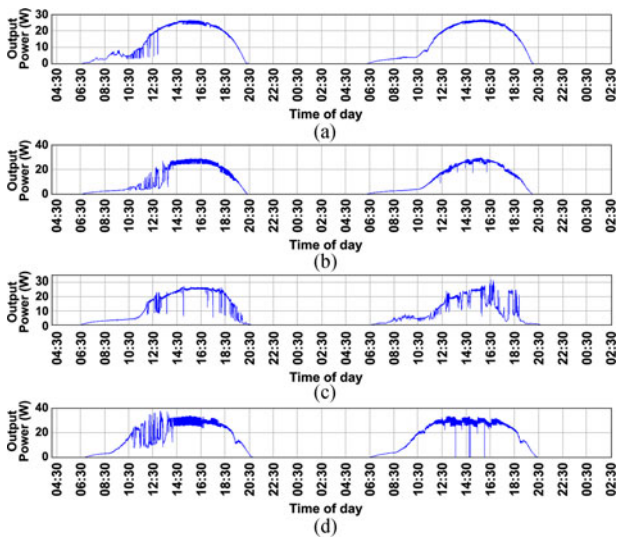

Fig. 6. Examples of the experimentally measured output power and battery voltage of: (a) configuration #1, (b) configuration #2, (c) configuration #3, and (d) configuration #4 in Table II.

tests, MPPT and battery charging regulation algorithms [3] were executed by the microcontroller-based energy management unit (see Fig. 1), which was incorporated in each power-supply system. The dc–dc converter drop to zero, that is observed in the second curve of Fig. 6(d), is due to the activation of the trickle-charging operating mode of the energy management control unit of the power-supply system, in order to prevent battery overcharging.

The individual power-supply systems employed in the experimental setup have been built using different devices (e.g., PV modules, batteries, etc.) of the same type, which, however, may exhibit a tolerance in their operational characteristics. In order to evaluate the performance of each power-supply configuration without being affected by this factor, the normalized energy conversion efficiency during the corresponding test period was calculated as follows:

$$n_{\text{eff}} = \sum_{i=1}^{T} (P_o(i) \cdot \Delta t) / \sum_{i=1}^{T} (P_{\text{PV}}(i) \cdot \Delta t) \qquad (19)$$

where $P_{\text{PV}}(i)$ and $P_o(i)$ are the dc–dc converter input and output power, respectively, at time step i, T is the total time duration of the corresponding experimental test, and Δt is the sampling period. The resulting normalized efficiency of the dc–dc converter in each configuration subject to the experimental evaluation process, as well as the total manufacturing cost of the corresponding RES-based power-supply system (includes the cost of PV modules, batteries, and dc–dc converter), is presented in Table III. These results also include the time intervals where the trickle-charging operating mode was activated. It is observed that the dc–dc converters in combinations #1 and #2 (see Table II), which have been optimally designed according to proposed methodology, feature a higher normalized efficiency by 11.95–12.01% compared to the nonoptimized dc–dc converter of configuration #3. Also, the normalized efficiency of the nonoptimized dc–dc converter in configuration #4 is lower by 12.10–12.16%

TABLE III
EXPERIMENTAL RESULTS IN TERMS OF NORMALIZED ENERGY CONVERSION EFFICIENCY AND COST

Configuration	PV array output energy (W·h)	DC–DC converter output energy (W·h)	Normalized efficiency (%)	Total manufacturing cost (€)
1	2084	1836	88.10	152.3
2	418	368	88.04	144.6
3	1560	1187	76.09	173.6
4	1301	988	75.94	201.6

compared to the optimized dc–dc converters of configurations #1 and #2. Furthermore, the partially optimized and totally nonoptimized RES-based power-supply systems (i.e., combinations #3 and #4 in Tables II and III) exhibit a total manufacturing cost which is higher by 13.9–39.4% than that of the RES systems in configurations #1 and 2, which have been designed by using the proposed optimization technique. Thus, the generated energy cost is higher for these configurations, compared to that of the totally (i.e., system- and circuit-level) optimized configurations derived by the proposed methodology. Finally, the optimized configurations #1 and #2, both comprising the same system-level-optimized RES structure (i.e., number of PV modules and batteries) but differing on the type of objective function applied during the circuit-level optimization stage, exhibited equivalent performance in terms of the dc–dc converter energy conversion efficiency. However, the total manufacturing cost (i.e., including the PV modules, batteries, and dc–dc converter) of configuration #2 is lower than that of #1 by 5.1%, since both the dc–dc converter cost and the impact of meteorological conditions at the target installation site during the year (affecting the yearly energy losses of the power converter) have been taken into account in the corresponding circuit-level design stage for calculating the LCOE objective function [see (13)]. Thus, the overall RES-based power-supply configuration #2 exhibits a lower cost of generated energy than configuration #1, where, similarly to past-proposed circuit-level design approaches, the dc–dc converter efficiency has been employed as a performance metric during the design phase.

V. CONCLUSION

In this paper, a new methodology has been presented for the optimal codesign of the RES-based power-supply structure of a WSN node simultaneously at the power-supply system level and the dc–dc converter circuit level, through a unified design process. The design optimization and experimental results demonstrated that by applying the power-supply system lifetime cost and the dc–dc converter circuit LCOE, respectively, as objective functions in the two stages of the proposed optimization process, then the resulting RES-based system is able to satisfy the energy requirements of the WSN node with a lower cost compared to that of partially optimized or totally nonoptimized power supplies. Thus, the cost of the WSN node is reduced accordingly. Furthermore, since WSNs typically comprise a large number of sensing nodes installed at different locations, the cost of the entire WSN is also reduced by using the proposed

design optimization method. Due to this benefit offered by the proposed technique, the work presented in this paper has been initially focused on the nodes of WSNs due to their extensive utilization during the last years in a wide variety of applications. However, future work also includes the evolution of the design technique presented in this paper (in terms of the power-supply topology, operation modeling, etc.) for the design optimization of any generic RES-based power-supply system that is used in either stand-alone or electric-grid-connected energy production installations.

Acknowledgment

The authors thank the administration and research/technical personnel of the Telecommunication Systems Research Institute (Technical University of Crete, Greece), as well as the administration and technical staff of "Georgios Liontas & Co. E.E." (Greece) for their contribution in conducting this research.

References

[1] G. Han, L. Liu, J. Jiang, L. Shu, and G. Hancke, "Analysis of energy-efficient connected target coverage algorithms for industrial wireless sensor networks," *IEEE Trans. Ind. Informat.*, vol. 13, no. 1, pp. 135–143, Feb. 2017.

[2] K. Sundareswaran, V. Vigneshkumar, P. Sankar, S. P. Simon, P. S. R. Nayak, and S. Palani, "Development of an improved P&O algorithm assisted through a colony of foraging ants for MPPT in PV system," *IEEE Trans. Ind. Informat.*, vol. 12, no. 1, pp. 187–200, Feb. 2016.

[3] E. Koutroulis and K. Kalaitzakis, "Novel battery charging regulation system for photovoltaic applications," *Proc. IEE—Elect. Power Appl.*, vol. 151, no. 2, pp. 191–197, 2004.

[4] W. Xu, Y. Zhang, Q. Shi, and X. Wang, "Energy management and cross layer optimization for wireless sensor network powered by heterogeneous energy sources," *IEEE Trans. Wireless Commun.*, vol. 14, no. 5, pp. 2814–2826, May 2015.

[5] F. Mansourkiaie, L. S. Ismail, T. M. Elfouly, and M. H. Ahmed, "Maximizing lifetime in wireless sensor network for structural health monitoring with and without energy harvesting," *IEEE Access*, vol. 5, pp. 2383–2395, Feb. 2017.

[6] M. Magno, D. Boyle, D. Brunelli, E. Popovici, and L. Benini, "Ensuring survivability of resource-intensive sensor networks through ultra-low power overlays," *IEEE Trans. Ind. Informat.*, vol. 10, no. 2, pp. 946–956, May 2014.

[7] J. Zhang, Z. Li, and S. Tang, "Value of information aware opportunistic duty cycling in solar harvesting sensor networks," *IEEE Trans. Ind. Informat.*, vol. 12, no. 1, pp. 348–360, Feb. 2016.

[8] Y. Li, Z. Jia, S. Xie, and F. Liu, "Dynamically reconfigurable hardware with a novel scheduling strategy in energy-harvesting sensor networks," *IEEE Sens. J.*, vol. 13, no. 5, pp. 2032–2038, May 2013.

[9] B. Zhang, R. Simon, and H. Aydin, "Harvesting-aware energy management for time-critical wireless sensor networks with joint voltage and modulation scaling," *IEEE Trans. Ind. Informat.*, vol. 9, no. 1, pp. 514–526, Feb. 2013.

[10] S. K. K. Ng, J. Zhong, and J. W. M. Cheng, "Probabilistic optimal sizing of stand-alone PV systems with modeling of variable solar radiation and load demand," in *Proc. Power Energy Soc. Gen. Meeting*, 2012, pp. 1–7.

[11] C. Paravalos, E. Koutroulis, V. Samoladas, T. Kerekes, D. Sera, and R. Teodorescu, "Optimal design of photovoltaic systems using high time-resolution meteorological data," *IEEE Trans. Ind. Informat.*, vol. 10, no. 4, pp. 2270–2279, Nov. 2014.

[12] M. Alsayed, M. Cacciato, G. Scarcella, and G. Scelba, "Multicriteria optimal sizing of photovoltaic-wind turbine grid connected systems," *IEEE Trans. Energy Convers.*, vol. 28, no. 2, pp. 370–379, Jun. 2013.

[13] B. J. Abdelhak, E. Najib, H. Abdelaziz, F. Hnaien, and F. Yalaoui, "Optimum sizing of hybrid PV/wind/battery using fuzzy-adaptive genetic algorithm in real and average battery service life," in *Proc. Int. Symp. Power Electron. Elect. Drives Autom. Motion*, 2014, pp. 871–876.

[14] O. H. Mohammed, Y. Amirat, M. Benbouzid, and A. A. Elbaset, "Optimal design of a PV/fuel cell hybrid power system for the city of Brest in France," in *Proc. 2014 Int. Conf. Green Energy*, 2014, pp. 119–123.

[15] M. Mirjafari, R. S. Balog, and R. Turan, "Multiobjective optimization of the DC-DC stage of a module-integrated inverter based on an efficiency usage model," *IEEE J. Photovolt.*, vol. 4, no. 3, pp. 906–914, May 2014.

[16] A. C. Nanakos, G. C. Christidis, and E. C. Tatakis, "Weighted efficiency optimization of flyback microinverter under improved boundary conduction mode (i-BCM)," *IEEE Trans. Power Electron.*, vol. 30, no. 10, pp. 5548–5564, Oct. 2015.

[17] G. Adinolfi, G. Graditi, P. Siano, and A. Piccolo, "Multiobjective optimal design of photovoltaic synchronous boost converters assessing efficiency, reliability, and cost savings," *IEEE Trans. Ind. Informat.*, vol. 11, no. 5, pp. 1038–1048, Oct. 2015.

[18] M. Kasper, D. Bortis, and J. W. Kolar, "Classification and comparative evaluation of PV panel-integrated DC-DC converter concepts," *IEEE Trans. Power Electron.*, vol. 29, no. 5, pp. 2511–2526, May 2014.

[19] F. Beltrame, F. H. Dupont, H. C. Sartori, E. C. Cancian, C. Rech, and J. R. Pinheiro, "Efficiency optimization of DC/DC boost converter applied to the photovoltaic system," in *Proc. 39th Annu. Conf. IEEE Ind. Electron. Soc.*, 2013, pp. 706–711.

[20] Y. Louvrier, P. Barrade, and A. Rufer, "Weight and efficiency optimization strategy of an interleaved DC-DC converter for a solar aircraft," in *Proc. 13th Eur. Conf. Power Electron. Appl.*, 2009, pp. 1–10.

[21] I. Mandourarakis and E. Koutroulis, "Design optimization of a RES-based power-supply system for wireless sensor networks," in *Proc. 2015 IEEE 15th Int. Conf. Environ. Elect. Eng.*, 2015, pp. 1–6.

[22] I. Mandourarakis and E. Koutroulis, "Optimal design of a boost-type DC-DC converter for PV power-supplied wireless sensor networks," in *Proc. 2015 IEEE Int. Conf. Ind. Technol.*, 2015, pp. 1100–1105.

[23] E. Lorenzo, *Solar Electricity—Engineering of Photovoltaic Systems*, 1st ed., PROGENSA, Sevilla, Spain, 1994.

[24] Z. Michalewicz, *Genetic Algorithms + Data Structures = Evolution Programs*, 2nd ed. New York, NY, USA: Springer, 1994.

[25] *Military Handbook 217-F: Reliability Prediction of Electronic Equipment*, Dept. Defense, Washington, DC, USA, 1991.

[26] S. E. De Leoán-Aldaco, H. Calleja, F. Chan, and H. R. Jimeánez-Grajales, "Effect of the mission profile on the reliability of a power converter aimed at photovoltaic applications—A case study," *IEEE Trans. Power Electron.*, vol. 28, no. 6, pp. 2998–3007, Jun. 2013.

[27] S. Burdakis, A. Inglezakis, and A. Deligiannakis, "Compressed data acquisition from water tanks," in *Proc. 1st ACM Int. Workshop Cyber-Phys. Syst. Smart Water Netw. Cyber Phys. Syst. Week*, Seattle, WA, USA, 2015, pp. 1–5.

[28] N. Mohan, T. M. Undeland, and W. P. Robbins, *Power Electronics: Converters, Applications, and Design*, 3rd ed. New York, NY, USA: Wiley, 2002.

Ioannis Mandourarakis received the Engineering Diploma and the M.Sc. degree in electronic and computer engineering from the Technical University of Crete, Chania, Greece, in 2011 and 2015, respectively, where he is currently working toward the Ph.D. degree in the School of Electrical and Computer Engineering, in the area of power electronics for photovoltaic energy production systems.

Eftichios Koutroulis (M'10–SM'15) was born in Chania, Greece, in 1973. He received the B.Sc. and M.Sc. degrees in electronic and computer engineering, in 1996 and 1999, respectively, and the Ph.D. degree in the area of power electronics and renewable energy sources (RES) from the School of Electronic and Computer Engineering, Technical University of Crete, Chania, in 2002.

He is currently an Associate Professor in the School of Electrical and Computer Engineering, Technical University of Crete. His research interests include power electronics, the development of microelectronic energy management systems for RES and the design of photovoltaic and wind energy conversion systems.